

# Quantum quenches in isolated quantum glasses out of equilibrium

S. J. Thomson,<sup>1,\*</sup> P. Urbani,<sup>1,†</sup> and M. Schiró<sup>1,‡</sup>

<sup>1</sup>*Institut de Physique Théorique, Université Paris Saclay, CNRS, CEA, F-91191 Gif-sur-Yvette, France*

(Dated: April 8, 2019)

In this work, we address the question of how a closed quantum system thermalises in the presence of a random external potential. By investigating the quench dynamics of the isolated quantum spherical  $p$ -spin model, a paradigmatic model of a mean-field glass, we aim to shed new light on this complex problem. Employing a closed-time Schwinger-Keldysh path integral formalism, we first initialise the system in a random, infinite-temperature configuration and allow it to equilibrate in contact with a thermal bath before switching off the bath and performing a quench. We find evidence that increasing the strength of either the interactions or the quantum fluctuations can act to lower the effective temperature of the isolated system and stabilise glassy behaviour.

*Introduction* - Investigating how physical systems react to external perturbations is a key tool in understanding their nature. Among physical perturbations, quenches play a central role in uncovering how many-body systems equilibrate [1], and when they fail to do so. The failure to equilibrate is of particular interest and has been the subject of a great deal of contemporary research. Understanding how and why many-body systems can fail to reach thermal equilibrium is not only of fundamental value (as it allows us to test the hypothesis underlying equilibrium statistical physics), but it also has practical applications: systems which fail to equilibrate can often exhibit rich new dynamical phenomena not seen in typical thermal states [2–5]

In recent years, two main mechanisms of ergodicity breaking in many-body quantum systems have emerged. On the one hand, quantum integrable systems have an extensive number of conserved charges and so do not thermalize to a state whose macroscopic properties are determined by only a few quantities (such as energy and density) [6]. On the other hand, there is also the many-body equivalent of Anderson localisation, *a.k.a.* Many Body Localization (MBL) [7–10]. In this case, the absence of thermalization is related to an *emergent* integrability [11]. However, unlike quantum integrable models that can be solved at (typically isolated) integrable points in the phase diagram, MBL systems display robust emergent integrability across the whole many-body localized phase. Several approaches have been proposed to construct the corresponding charges or (local) integrals of motions [12–14].

Both integrable and MBL systems display strong ergodicity breaking in the sense that their unitary dynamics never reach a thermal state on any timescale. However, in between systems that are able to thermalize and the ones that are not, there is a huge class of systems for which thermalization is possible but only on very long timescales. These are glassy systems, whose dynamics display ergodicity breaking due to metastability. In this case, the dynamical evolution is trapped by exponentially many metastable states that forbid equilibration on short timescales. In finite dimensions, such metastable states

have a finite (but very long) lifetime, while in the mean field limit their lifetime diverges with the system size (or dimension) due to the divergence of the free energy barriers between them. Nevertheless those systems are never completely out of equilibrium since in the end they relax on timescales that scale exponentially in either the system size or dimension [15, 16].

In contrast with MBL and integrable systems, glassy systems do not depend crucially on isolation from their environment or the presence of quenched disorder. Instead, the crucial feature is the roughness of the emerging free energy landscape which is robust both when the temperature is finite but low enough and independently of whether quenched disorder is present [17, 18]. The dynamical behavior of quantum glasses has been extensively studied in recent years, either motivated by the idea of a disorder-free localization [19–24] or through the solution of simplified models which are mean field in nature. In this case, the analysis has been mainly performed in a dissipative setting [25–30] where such models are coupled to thermal environments, or limited to small systems sizes through exact numerical studies of eigenstate properties [31–33], leaving out the question of what happens in the thermodynamic limit when the system evolves under its own closed dynamical evolution without any coupling to the bath.

In this work we address this question by focusing on the unitary dynamics of the isolated spherical quantum  $p$ -spin model, a paradigmatic example of a mean-field glass, whose Hamiltonian

$$\mathcal{H} = \frac{1}{2m} \sum_i \Pi_i^2 - \mathcal{J}(t) \sum_{i_1 < \dots < i_p} J_{i_1 \dots i_p} \sigma_{i_1} \dots \sigma_{i_p} \quad (1)$$

describes a set of spins  $\sigma_i$  all-to-all coupled by random  $p$ -body interactions  $J_{i_1 \dots i_p}$  drawn from a Gaussian distribution with zero mean and unit variance. In order to make the model more tractable but still non-trivial, we treat the spins as continuous variables [34] and enforce the spherical constraint  $\sum_i \sigma_i^2 = N$  by adding a Lagrange multiplier (hereafter denoted  $z$ ). We further add a conjugate momentum  $\Pi_i$  where  $[\Pi_i, \sigma_j] = i\hbar(t)\delta_{ij}$

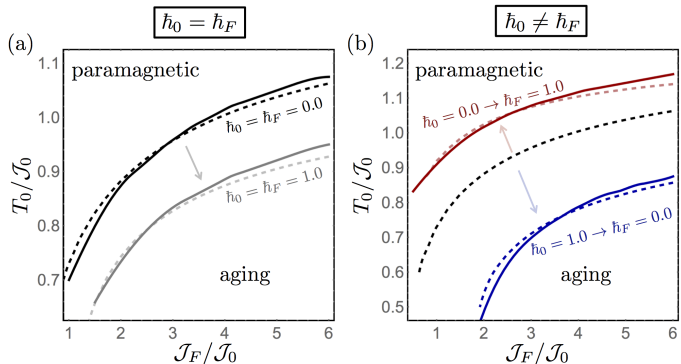


FIG. 1: Non-equilibrium phase diagram, starting from an initial temperature  $T_0$ . The system is first equilibrated in contact with a thermal bath before cutting off the bath and performing a quench in both the strength of the random interactions and quantum fluctuations,  $(\mathcal{J}_0, \hbar_0) \rightarrow (\mathcal{J}_F, \hbar_F)$ . The boundary between the paramagnetic and aging regime shifts and displays a strong dependence on the strength of quantum fluctuations, both before and after the quench. In particular, when quantum fluctuations are kept constant throughout the quench, i.e.  $\hbar_0 = \hbar_F$ , the aging regime is suppressed as compared to the classical case (left panel). As opposite, when quantum fluctuations are suddenly increased (decreased) the aging regime is enhanced (suppressed) as compared to the classical case (right panel). Details of how the boundaries were obtained are given in the main text.

are canonical commutation relations, and we allow  $\hbar(t)$  to be time-dependent in order to be able to change the strength of quantum fluctuations - for details, see the Supplementary Material [35]. This model has been extensively studied in both its classical version [17, 36–42] as well as in its quantum guise when coupled to a thermal bath [25–27, 29, 43–45]. At low temperature, the model displays a *dynamical* glass transition  $T_d$  due to the emergence of long-lived glassy states. Below this temperature equilibration is never reached and the system ages forever (but not on exponential timescales). The dynamical temperature is a decreasing function of the strength of quantum fluctuations, as one may expect [26]. Though the isolated dynamics of the quantum  $p$ -spin model have not previously been studied, the classical isolated dynamics was recently investigated in [46]. Here we study the unitary *quantum* evolution of this model: we prepare a typical initial configuration at some temperature  $T_0$  in the paramagnetic phase and then we suddenly change both the strength of the random couplings  $\mathcal{J}(t)$  and the strength of quantum fluctuations measured by  $\hbar(t)$ , keeping the system isolated. The resulting non-equilibrium phase diagram, plotted in Figure 1, features a high-temperature paramagnetic phase, where the system relaxes toward equilibrium, and a low-temperature phase where aging and breakdown of time-translational invariance emerge. Surprisingly, we find that the phase

boundary between the paramagnetic and aging regimes strongly depends on whether quantum fluctuations are suddenly changed (right panel) or kept constant throughout the evolution (left panel). In particular we find that a sudden increase of quantum fluctuations promotes rather suppresses glassy effects (right panel, top curve), in striking contrast to what is expected from the equilibrium phase diagram. On the other hand, when the strength of quantum fluctuations is kept constant (left panel, bottom curve) the aging regime in the quantum model shrinks with respect to its classical counterpart, as expected thermodynamically. The resulting picture is that of an enhanced aging regime due to the interplay of quantum fluctuations and non-equilibrium effects. We interpret this intriguing result in terms of an effective temperature  $T_{eff} < T_0$  for the isolated disordered quantum system, which in the absence of an external thermal bath is able to cool itself down through quantum fluctuations, eventually crossing the glass transition.

*Dynamical Equations for Correlation and Response* - Throughout this work we will focus in particular on the dynamics of correlation and response functions, which are defined by

$$C(t, t') = \frac{1}{2} \langle [\sigma(t), \sigma(t')]_+ \rangle \quad (2)$$

$$R(t, t') = \theta(t - t') \frac{i}{\hbar(t')} \langle [\sigma(t), \sigma(t')]_- \rangle \quad (3)$$

where  $[A, B]_{\pm} = AB \pm BA$ . The dynamics of the model can be completely solved using the Keldish formalism [47]. The fully connected nature of the model defined in Eq. (1) allows us to derive closed dynamical equations that describe the evolution of correlation and response functions starting from an uncorrelated infinite temperature initial state. After disorder-averaging and taking the  $N \rightarrow \infty$  limit, the equations of motion for the correlation and response functions can be obtained following the method of Ref. [43] and are given by

$$[m\partial_t^2 + z(t)]R(t, t') = \delta(t - t') + \int_0^\infty dt'' \Sigma(t, t'')R(t'', t) \quad (4)$$

$$[m\partial_t^2 + z(t)]C(t, t') = \int_0^\infty dt'' \Sigma(t, t'')C(t'', t') + \int_0^{t'} dt'' D(t, t'')R(t', t'') \quad (5)$$

where we have defined the self-energies  $\Sigma(t, t')$  and  $D(t, t')$  as:

$$\Sigma(t, t') = -\frac{p\mathcal{J}(t)\mathcal{J}(t')}{\hbar(t')} \text{Im} \left[ C(t, t') - \frac{i\hbar(t')}{2} R(t, t') \right]^{p-1} \quad (6)$$

$$D(t, t') = \frac{p\mathcal{J}(t)\mathcal{J}(t')}{2} \times \text{Re} \left[ C(t, t') - \frac{i}{2} (\hbar(t')R(t, t') + \hbar(t)R(t', t)) \right]^{p-1} \quad (7)$$

We notice that with respect to the classical dynamical equations [46], Eqs. (6-7) have extra self-energy contributions proportional to  $\hbar(t)$  which arise from purely quantum fluctuations [25]. We perform the dynamical evolution subject to a time-dependent Lagrange multiplier  $z(t)$  which is used to enforce the global spherical constraint. We can derive the dynamical equation for this by taking the equal-time limit of Eq. 5 to obtain [43]:

$$z(t) = \int_0^t dt'' [\Sigma(t, t'')C(t'', t) + D(t, t'')R(t, t'')] - m\partial_t^2 C(t, t')|_{t' \rightarrow t-} \quad (8)$$

Equations 4,5 and 8 are the three dynamical equations which we will base the rest of this paper on. They have a causal structure and therefore they can be straightforwardly discretised and solved numerically - for further details, see the Supplementary Material [35].

*Finite Temperature Initial State Preparation and Double Quench* - The dynamical equations (4,5 and 8) describe the evolution of the system from an initial infinite temperature initial state uncorrelated with the disorder. Here we are instead interested in studying dynamics from an initial finite temperature state. Within the Keldysh formalism this would require formulating the dynamical equations on a three branch contour corresponding to imaginary time, as recently proposed in [48]. To avoid the complexities of this approach, we instead perform the initial thermalisation numerically through a double-quench protocol. Specifically, we first quench from infinite temperature to some  $T_0 > T_d$  and  $\mathcal{J}(0 < t < t_q) \equiv \mathcal{J}_0 = 1$  and  $\hbar(0 < t < t_q) \equiv \hbar_0$  and allow the system to thermalise in contact with a thermal bath, which we assume to be a set of harmonic oscillators in thermal equilibrium at some temperature  $T_0$ , as in Ref. 25. This results in modified self-energies  $\tilde{\Sigma}(t, t')$  and  $\tilde{D}(t, t')$  in Eq. 7 due to the bath coupling, whose explicit expressions are given in [35]. Then, for  $t > t_q$  we switch off the coupling to the bath and let the system evolve unitarily with  $\mathcal{J}(t \geq t_q) \equiv \mathcal{J}_F$  and  $\hbar(t > t_q) \equiv \hbar_F$ . All temperatures are measured in units of  $\mathcal{J}_0$ . Supporting data demonstrating that our system is well-equilibrated to the bath temperature is shown in Supplementary Material [35].

*Results* - For concreteness we will set  $p = 3$ , though we expect our results to hold for any  $p > 2$ . In Fig. 2 we plot the dynamics of correlation function  $C(\tau + t_w, t_w)$  at fixed  $\mathcal{J}_0 = 1$  for different type of quenches. First we notice (top panel) that upon increasing the strength of quantum fluctuations the dynamics slows down and a plateau in the correlation function begins to emerge as  $\hbar_F$  increases from zero. Such a plateau is associated with a non-zero Edwards-Anderson glassy order parameter. On the contrary, the inset plot in the same panel shows how a decreasing  $\hbar_F < \hbar_0$  makes the system thermalize more rapidly. In the central panel we plot the

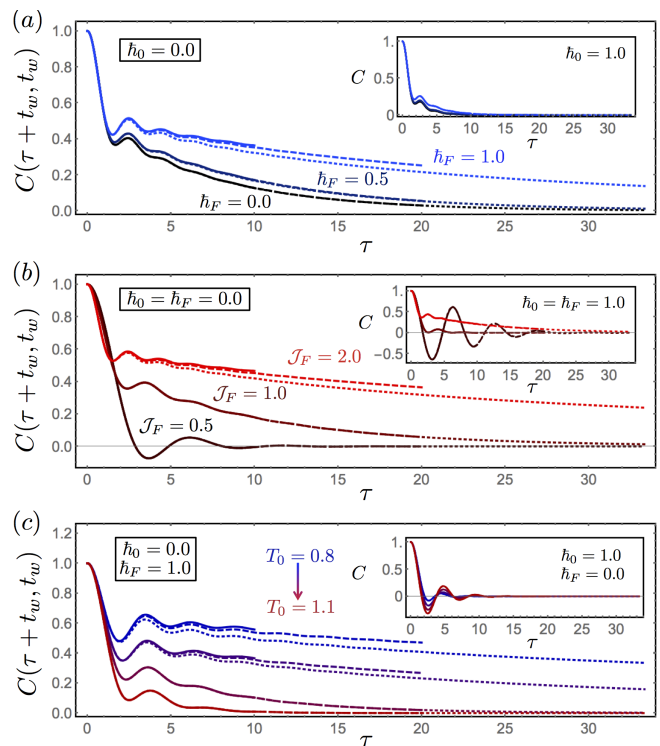


FIG. 2: Correlation functions after the second quench for a variety of different parameters, with  $N = 15000$  steps,  $t_{max} = 100$  and  $t_q = t_{max}/2$ . In each case,  $\mathcal{J}_0 = 1.0$  and the wait times are  $t_w = 16.67$  (dotted),  $t_w = 30$  (dashed) and  $t_w = 40$  (solid). a) The effects of quantum fluctuations on a system prepared at  $T_0 = 1.0$  with  $\hbar_0 = 0.0$  and  $\mathcal{J}_F = 2$ . A plateau emerges as  $\hbar_F$  is increased. Inset: the same quantities for a system prepared with  $\hbar_0 = 1.0$ . b) The effects of quenches in  $\mathcal{J}$  on the dynamics of a state with  $T_{bath} = 0.8$  and  $\hbar_0 = \hbar_F = 0.0$ : quenches with  $\mathcal{J}_F > \mathcal{J}_0$  pump energy into the system, while quenches with  $\mathcal{J}_F < \mathcal{J}_0$  extract energy and can lead to aging behaviour. Inset: the same quantities for a system prepared with  $\hbar_0 = 1.0$ . c) A comparison of the initial bath temperatures on the dynamics of a state with  $\hbar_0 = 0$  and  $\hbar_F = 1$  and  $\mathcal{J}_F = \mathcal{J}_0 = 1$ . Aging behaviour is visible at temperatures higher than the equilibrium transition temperature  $T_d \approx 0.6$ . Inset: the same quantities for the quench  $\hbar_0 = 1.0 \rightarrow \hbar_F = 0.0$ .

dependence of the dynamics from the interaction quench at fixed  $\hbar_0 = \hbar_F = 0.0$ , resulting in an enhanced plateau for  $\mathcal{J}_F > \mathcal{J}_0$ , while a faster relaxation toward equilibrium emerges for  $\mathcal{J}_F < \mathcal{J}_0$ , with a related behavior emerging in the quantum case  $\hbar_0 = \hbar_F = 1$  (see inset). Finally, we study the quench dynamics at fixed  $\mathcal{J}_F = \mathcal{J}_0$  for different values of the bath temperature (bottom panel). We find that cooling the system strengthens the plateau and enhance the waiting time dependence. We remark that for the timescales accessible to our current simulations, the correlation function still decays and does not display a true plateau: this is likely an effect of not being able to access sufficiently long waiting times  $t_w$  to see the true

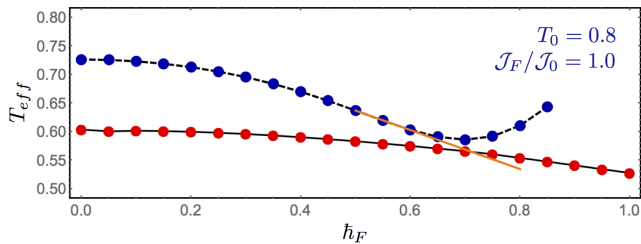


FIG. 3: Red: The equilibrium phase boundary, as obtained numerically using a single quench from infinite temperature with  $N = 15000$  steps and  $t_{max} = 100$ . Blue: The effective temperature after the second quench for a system initially equilibrated at  $T_{bath} = 0.8$  and  $\mathcal{J}_F = \mathcal{J}_0 = 1.0$ , also with  $N = 15000$  and  $t_{max} = 100$ , with  $t_q = t_{max}/2$ . As the strength of quantum fluctuations is increased, the effective temperature of the system decreases until it reaches approximately the equilibrium transition temperature, here at a value  $\hbar_F \approx 0.7$ . Beyond this,  $T_{eff}$  displays the same non-monotonic behaviour seen in Ref. 46, indicating a violation of FDT and suggesting that the system has entered the glass phase.

plateau, as evidenced by the strengthening of the plateau for larger  $t_w$ . By approximating  $C(\tau + t_w, t_w)|_{\tau \rightarrow \infty}$  by the value of the correlation function at the longest times accessible to our simulation, and identifying this value with the Edwards-Anderson order parameter  $q_{EA}$ , we can plot an approximate non-equilibrium phase diagram for the isolated quantum system, shown in Fig. 1. Within our simulation times, as clearly shown by Fig. 2, we cannot reach the true  $t \rightarrow \infty$  value of  $q_{EA}$ . Instead, we can set a threshold value and approximate that all  $q \leq q_{th}$  are slowly decaying paramagnetic solutions, whereas for  $q > q_{th}$  the system is in a true glassy phase. The results of this are shown in the phase diagram in Fig. 1 by dashed lines, using  $q_{th} \approx 0.2$ , though the qualitative shape of the phase diagram does not depend strongly on this choice [54].

*Effective Temperature and Quench-Induced Cooling* - The results presented above indicate that quantum fluctuations and non-equilibrium effects can strongly enhance glassiness and increase the region of parameters where aging effects are observed. This is surprising at first, since glassiness is a low temperature property, while exciting the system with a global quantum quench injects extensive energy and should intuitively induce heating, as often observed in quantum quench studies [49, 50]. In order to understand the physical origin of this effect it is instructive to consider the effective temperature at which the isolated system thermalizes after the unitary time evolution following the switch-off of the thermal bath. This can be estimated from the fluctuation-dissipation relation, as we discuss in the SM. In general terms one could expect that after a global quantum quench the system would thermalize to a larger effective tempera-

ture. As we show in Fig. 3 this is not the case when the strength of quantum fluctuations is increased, but rather the effective temperature *decreases* with  $\hbar_F$  and eventually crosses the dynamical critical temperature of the equilibrium problem, resulting in an enhanced aging behavior. A decrease of the effective temperature with quantum fluctuations can be also rationalized from an energetic argument. Indeed the effective temperature roughly corresponds to the temperature at which the internal energy matches the energy of the initial state, conserved during the unitary evolution. Upon increasing quantum fluctuations the internal energy increases, i.e. the classical paramagnetic state has lower energy. By extracting the local minimum of  $T_{eff}$  and identifying it with the transition in our numerical data, we can draw a phase boundary with no free parameters, shown in Fig. 1 by the solid lines.

*Conclusions* - In this work we have studied the quench dynamics of an isolated quantum glass. Remarkably, we have shown that suddenly increasing the strength of quantum fluctuations enhances aging behavior, in contradiction with common expectations based on the physics of quantum glasses coupled to thermal environment. The key feature of this effect relies on the possibility of the isolated quantum system to lower its own temperature due to the effect of quantum fluctuations. Therefore our results suggest that quantum fluctuations in isolated, interacting, disordered systems can indeed favour glassy behaviour and ergodicity breaking. For future work, it would be beneficial to confirm the results obtained here by performing the initial equilibration step analytically, likely by adding a third branch to the Keldysh contour corresponding to imaginary time and performing the disorder average using the replica trick. The corresponding dynamical equations for a quench of disordered interactions are already available in [51] and this may ultimately even allow the system to be initialised at  $T < T_d$ , letting us study the dynamics of an equilibrium glass state when quenched in different ways. In addition, our analysis relies on the assumptions that the timescales over which we look at the evolution of the system are  $\sim \mathcal{O}(1)$  with respect to  $N$  (since they are obtained via a saddle point approximation). It would be very interesting to understand what happens on larger timescales, and whether the aging we see here persists to timescales exponentially long relative to the system size. Finally, it would be worth extending similar real-time dynamical studies to other mean field models of quantum glasses, including the Ising  $p$ -spin and the quantum Random Energy Model whose properties in absence of a thermal bath have been recently investigated [52, 53].

We acknowledge helpful discussions with L. Cugliandolo and M. Tarzia. This work was supported by the grant Investissements d’Avenir from LabEx PALM (ANR-10-LABX-0039-PALM), the grant DynDisQ from DIM SIRTEQ and by the CNRS through the PICS-USA-

14750. The majority of the computations were performed on the Collège de France IPH cluster computer.

---

\* Electronic address: steven.thomson@ipht.fr

† Electronic address: pierfrancesco.urbandi@ipht.fr

‡ Electronic address: marco.schiro@ipht.fr

- [1] A. M. Kaufman, M. E. Tai, A. Lukin, M. Rispoli, R. Schittko, P. M. Preiss, and M. Greiner, *Science* **353**, 794 (2016).
- [2] T. Kinoshita, T. Wenger, and D. S. Weiss, *Nature* **440**, 900 (2006).
- [3] M. Gring, M. Kuhnert, T. Langen, T. Kitagawa, B. Rauer, M. Schreitl, I. Mazets, D. A. Smith, E. Demler, and J. Schmiedmayer, *Science* **337**, 1318 (2012).
- [4] D. Fausti, R. I. Tobey, N. Dean, S. Kaiser, A. Dienst, M. C. Hoffmann, S. Pyon, T. Takayama, H. Takagi, and A. Cavalleri, *Science* **331**, 189 (2011).
- [5] M. Mitrano, A. Cantaluppi, D. Nicoletti, S. Kaiser, A. Perucchi, S. Lupi, P. Di Pietro, D. Pontiroli, M. Riccò, S. R. Clark, et al., *Nature* **530**, 461 (2016).
- [6] F. H. Essler and M. Fagotti, *Journal of Statistical Mechanics: Theory and Experiment* **2016**, 064002 (2016).
- [7] D. Basko, I. Aleiner, and B. Altshuler, *Annals of Physics* **321**, 1126 (2006), ISSN 0003-4916.
- [8] R. Nandkishore and D. A. Huse, *Annu. Rev. Condens. Matter Phys.* **6**, 15 (2015).
- [9] F. Alet and N. Laflorencie, *Comptes Rendus Physique* **19**, 498 (2018), ISSN 1631-0705, quantum simulation / Simulation quantique.
- [10] D. A. Abanin, E. Altman, I. Bloch, and M. Serbyn, arXiv e-prints arXiv:1804.11065 (2018), 1804.11065.
- [11] D. A. Huse, R. Nandkishore, and V. Oganesyan, *Physical Review B* **90**, 174202 (2014).
- [12] V. Ros, M. Müller, and A. Scardicchio, *Nuclear Physics B* **891**, 420 (2015).
- [13] C. Monthus, *Journal of Statistical Mechanics: Theory and Experiment* **2016**, 033101 (2016).
- [14] S. J. Thomson and M. Schiró, *Phys. Rev. B* **97**, 060201 (2018).
- [15] T. Castellani and A. Cavagna, *Journal of Statistical Mechanics: Theory and Experiment* **2005**, P05012 (2005).
- [16] A. Cavagna, *Physics Reports* **476**, 51 (2009).
- [17] L. F. Cugliandolo and J. Kurchan, *Phys. Rev. Lett.* **71**, 173 (1993).
- [18] P. Charbonneau, J. Kurchan, G. Parisi, P. Urbani, and F. Zamponi, *Annual Review of Condensed Matter Physics* **8**, 265 (2017).
- [19] G. Carleo, F. Becca, M. Schiró, and M. Fabrizio, ArXiv e-prints (2011), 1109.2516.
- [20] T. Grover and M. P. A. Fisher, *Journal of Statistical Mechanics: Theory and Experiment* **2014**, P10010 (2014).
- [21] Z. Papi, E. M. Stoudenmire, and D. A. Abanin, *Annals of Physics* **362**, 714 (2015), ISSN 0003-4916.
- [22] M. van Horssen, E. Levi, and J. P. Garrahan, *Phys. Rev. B* **92**, 100305 (2015).
- [23] N. Y. Yao, C. R. Laumann, J. I. Cirac, M. D. Lukin, and J. E. Moore, *Phys. Rev. Lett.* **117**, 240601 (2016).
- [24] A. Smith, J. Knolle, D. L. Kovrizhin, and R. Moessner, *Phys. Rev. Lett.* **118**, 266601 (2017).
- [25] L. F. Cugliandolo and G. Lozano, *Phys. Rev. B* **59**, 915 (1999).
- [26] L. F. Cugliandolo, D. R. Grempel, and C. A. da Silva Santos, *Phys. Rev. B* **64**, 014403 (2001).
- [27] L. F. Cugliandolo, D. R. Grempel, G. Lozano, H. Lozza, and C. A. da Silva Santos, *Phys. Rev. B* **66**, 014444 (2002).
- [28] G. Biroli and O. Parcollet, *Phys. Rev. B* **65**, 094414 (2002).
- [29] L. F. Cugliandolo, D. R. Grempel, G. Lozano, and H. Lozza, *Phys. Rev. B* **70**, 024422 (2004).
- [30] T. E. Markland, J. A. Morrone, B. J. Berne, K. Miyazaki, E. Rabani, and D. R. Reichman, *Nature Physics* **7**, 134 EP (2011).
- [31] C. R. Laumann, A. Pal, and A. Scardicchio, *Phys. Rev. Lett.* **113**, 200405 (2014).
- [32] C. L. Baldwin, C. R. Laumann, A. Pal, and A. Scardicchio, *Phys. Rev. B* **93**, 024202 (2016).
- [33] C. L. Baldwin, C. R. Laumann, A. Pal, and A. Scardicchio, *Phys. Rev. Lett.* **118**, 127201 (2017).
- [34] J. M. Kosterlitz, D. J. Thouless, and R. C. Jones, *Phys. Rev. Lett.* **36**, 1217 (1976).
- [35] (????), see the Supplementary Material at [link].
- [36] B. Derrida, *Phys. Rev. Lett.* **45**, 79 (1980).
- [37] B. Derrida, *Phys. Rev. B* **24**, 2613 (1981).
- [38] D. Gross and M. Mezard, *Nuclear Physics B* **240**, 431 (1984), ISSN 0550-3213.
- [39] T. R. Kirkpatrick and D. Thirumalai, *Phys. Rev. Lett.* **58**, 2091 (1987).
- [40] T. R. Kirkpatrick and D. Thirumalai, *Phys. Rev. B* **36**, 5388 (1987).
- [41] A. Crisanti, H. Horner, and H. J. Sommers, *Zeitschrift für Physik B Condensed Matter* **92**, 257 (1993), ISSN 1431-584X.
- [42] T. Castellani and A. Cavagna, *Journal of Statistical Mechanics: Theory and Experiment* **2005**, P05012 (2005).
- [43] L. F. Cugliandolo and G. Lozano, *Phys. Rev. Lett.* **80**, 4979 (1998).
- [44] G. Biroli and L. F. Cugliandolo, *Phys. Rev. B* **64**, 014206 (2001).
- [45] L. F. Cugliandolo, G. Lozano, and H. Lozza, *The European Physical Journal B - Condensed Matter and Complex Systems* **41**, 87 (2004).
- [46] L. F. Cugliandolo, G. S. Lozano, and E. N. Nessi, *Journal of Statistical Mechanics: Theory and Experiment* **2017**, 083301 (2017).
- [47] A. Kamenev, *Field theory of non-equilibrium systems* (Cambridge University Press, 2011).
- [48] L. F. Cugliandolo, G. S. Lozano, and N. Nessi, arXiv e-prints arXiv:1811.03987 (2018), 1811.03987.
- [49] A. Mitra and T. Giamarchi, *Phys. Rev. Lett.* **107**, 150602 (2011).
- [50] M. Schiró and A. Mitra, *Phys. Rev. Lett.* **112**, 246401 (2014).
- [51] L. F. Cugliandolo, G. S. Lozano, and N. Nessi, *Journal of Statistical Mechanics: Theory and Experiment* **2019**, 023301 (2019).
- [52] L. Faoro, M. Feigel'man, and L. Ioffe, arXiv e-prints arXiv:1812.06016 (2018), 1812.06016.
- [53] M. Tarzia, to appear (2019).
- [54] To extract the true phase boundary one would need to consider the relaxation time of the system as a function of the control parameters and try to fit its divergence, however the timescales required to perform this analysis are longer than accessible with our numerical code.

# Supplementary Material to “Quantum quenches in isolated quantum glasses out of equilibrium”

S. J. Thomson,<sup>1</sup> P. Urbani,<sup>1</sup> and M. Schiró<sup>1</sup>

<sup>1</sup>*Institut de Physique Théorique, Université Paris Saclay, CNRS, CEA, F-91191 Gif-sur-Yvette, France*

(Dated: April 8, 2019)

In this Supplementary Material, we provide additional technical details about the derivation of the dynamical equations, the numerical procedure used to solve the dynamical equations and additional data confirming that the initial equilibration phase of our double-quench procedure performs as expected.

## I. DERIVATION OF THE DYNAMICAL EQUATIONS

### A. Linear Response

In order to allow the strength of quantum fluctuations in this calculation to be parametrised by a time-dependent  $\hbar(t)$ , we must be precise about how this time-dependence enters in the various quantities which we are interested in computing. In particular, to define the response function in the presence of a time-dependent  $\hbar(t)$ , we must first revisit linear response theory. Defining the Schrödinger equation as  $i\hbar(t)\partial_t\psi(t) = \hat{\mathcal{H}}\psi(t)$ , linear response theory leads to the definition:

$$R(t, t') = \frac{i}{\hbar(t')} \Theta(t - t') \langle [O(t), O(t')] \rangle \quad (1)$$

where the  $\hbar(t')$  in the response function takes the earlier of the two time arguments, and  $O(t)$  represents an arbitrary local observable. This will be important in evaluating the saddle-point equations of the disorder-averaged action.

### B. Generating Functional

The generating functional can be written as:

$$\mathcal{Z}[\xi^+, \xi^-] = \int \mathcal{D}\sigma^+ \mathcal{D}\sigma^- \exp \left[ i \left( \tilde{S}[\sigma^+] - \tilde{S}[\sigma^-] + \int \frac{dt}{\hbar(t)} (\xi^+(t)\sigma^+(t) - \xi^-(t)\sigma^-(t)) \right) \right] \langle \sigma + |\rho(0)|\sigma^- \rangle \quad (2)$$

where  $\rho(0)$  represents the element of the initial density matrix at  $t = 0$  and is chosen to be uncorrelated with the disorder (i.e. a random, infinite-temperature initial state). The tilde notation signifies that the time-dependent factors of  $1/\hbar(t)$  have been absorbed into the definition of the action and appear under the relevant time integrals. The action  $\tilde{S}$  can be defined in terms of a quadratic term  $S_0$  and a disordered interaction term  $V[\sigma, J]$ :

$$\tilde{S}_s[\sigma, J] = \tilde{S}_0[\sigma] - \int_0^\infty \frac{dt}{\hbar(t)} V[\sigma, J], \quad (3)$$

$$\tilde{S}_0[\sigma] = \int_0^\infty \frac{dt}{\hbar(t)} \left[ \frac{m}{2} \dot{\sigma}^2 - \frac{z}{2} (\sigma^2 - N) \right], \quad (4)$$

$$V[\sigma, J] = \mathcal{J}(t) \sum_{i_1 < \dots < i_p}^N J_{i_1 \dots i_p} \sigma_{i_1} \dots \sigma_{i_p}. \quad (5)$$

The quadratic part  $S_0$  contains a kinetic term, chosen such that the eventual dynamical equations are written in terms of second derivatives with respect to time. In the presence of the global spherical constraint that enforces  $\sum_i^N \sigma_i^2 = N$  through the introduction of a Lagrange multiplier  $z$ , the variables  $\sigma_i$  are real, continuous dynamic variables constrained to lie between  $-\sqrt{N} < \sigma_i < \sqrt{N} \forall i$ .

This action can be split into components  $\sigma^+$  and  $\sigma^-$  residing on the forward and backwards Keldysh contours respectively, to give an action:

$$\tilde{S}[\sigma^+, \sigma^-, J] = \tilde{S}_0[\sigma^+] - \tilde{S}_0[\sigma^-] - \int_0^\infty \frac{dt}{\hbar(t)} (V[\sigma^+, J] - V[\sigma^-, J]) \quad (6)$$

where the relative minus sign comes from reversing the integration limits on the reverse contour. For clarity, in the following we will drop the tilde notation, but it is to be understood that the time-dependent  $\hbar(t)$  remains under the relevant integrals in all of the following expressions.

### C. System-Bath Coupling

The coupling between the system and bath can be treated exactly as in Ref. 1. The time-dependent  $\hbar(t)$  presents no complications, as we switch off the system-bath coupling at a time  $t_q$ , defined as a time where the system has initially equilibrated with the thermal bath. Therefore, all factors of  $\hbar(t)$  can simply be replaced by  $\hbar_0$  in the following expressions. We couple the quantum  $p$ -spin Hamiltonian linearly to a bath of harmonic oscillators assumed to be in thermal equilibrium. This coupling can be described by the Feynman-Vernon influence functional:

$$S_{bath} = \frac{1}{\hbar_0} \int_0^{t_q} dt \int_0^{t_q} dt' (-[\sigma^+(t) - \sigma^-(t)]\eta(t-t')[\sigma^+(t') + \sigma^-(t')] + i[\sigma^+(t) - \sigma^-(t)]\nu(t-t')[\sigma^+(t') - \sigma^-(t')]) \quad (7)$$

where  $\eta$  and  $\nu$  are the correlation and response functions of the bath, and are time-translation invariant due to the bath being in equilibrium. They are given by:

$$\eta(t-t') = -\Theta(t-t') \int_0^\infty d\omega I(\omega) \sin[\omega(t-t')], \quad (8)$$

$$\nu(t-t') = \int_0^\infty I(\omega) \coth\left(\frac{1}{2}\beta\hbar_0\omega\right) \cos[\omega(t-t')] \quad (9)$$

where  $I(\omega)$  is the spectral function of the bath. We choose an Ohmic bath with  $I(\omega) = \frac{1}{\pi} \exp(-|\omega|/\Lambda)$ , for which explicit expressions for both  $\nu(t-t')$  and  $\eta(t-t')$  can be straightforwardly found, and we choose the integration cutoff to be  $\Lambda = 5$ .

### D. Disorder Averaging

Under the assumption that  $\hat{\rho}(0)$  is uncorrelated with the disorder, we can perform the disorder average explicitly. Assuming the distribution of the disorder variable  $J_{i_1\dots i_p}$  is given by a Gaussian with zero mean and variance of the form:

$$P[J] = \sqrt{\frac{N^{p-1}}{\pi p!}} \exp\left(-\frac{N^{p-1}}{p!} \sum_{i_1 \neq \dots \neq i_p} (J_{i_1\dots i_p})^2\right) \quad (10)$$

such that

$$\overline{(J_{i_1\dots i_p})^2} = \int dJ P[J] (J_{i_1\dots i_p})^2 = \frac{p!}{2N^{p-1}} \quad (11)$$

where the factors of  $N$  and  $p$  are included to simplify later expressions. The prefactor  $\mathcal{J}(t)$  shown in the main text therefore acts as a time-dependent disorder strength that we can use in the double-quench procedure. The average of any operator is given by:

$$\overline{\langle \sigma(t) \rangle} \equiv \left. \frac{\partial \ln \mathcal{Z}[\xi^+, \xi^-, J]}{\partial \xi^+(t)} \right|_{\xi=0} = \frac{1}{\mathcal{Z}[0, 0, J]} \left. \frac{\partial \mathcal{Z}[\xi^+, \xi^-, J]}{\partial \xi^+(t)} \right|_{\xi=0} \quad (12)$$

from which it follows that the only averaging to be done is over  $\mathcal{Z}$  itself rather than  $\ln \mathcal{Z}$ . The disorder average therefore reduces to just averaging over the  $p$ -spin vertex, the only term to have a disorder dependence. It can be performed explicitly to give a disorder-averaged generating functional:

$$\overline{\mathcal{Z}[\xi^+, \xi^-, J]} = \int \mathcal{D}_{\sigma^-} \mathcal{D}_{\sigma^+} \exp\left[i\left(S_{eff}[\sigma^+, \sigma^-] + \int dt (\xi^+(t)\sigma^+(t) - \xi^-(t)\sigma^-(t))\right)\right] \quad (13)$$



with the disorder-averaged effective action:

$$S_{eff}[\boldsymbol{\sigma}^+, \boldsymbol{\sigma}] = S_0[\boldsymbol{\sigma}^+] - S_0[\boldsymbol{\sigma}^-] - V_D[\boldsymbol{\sigma}^+, \boldsymbol{\sigma}^-] + S_{bath}[\boldsymbol{\sigma}^+, \boldsymbol{\sigma}], \quad (14)$$

$$V_D[\boldsymbol{\sigma}^+, \boldsymbol{\sigma}^-] = \frac{iN}{4} \int dt dt' \frac{\mathcal{J}(t)\mathcal{J}(t')}{\hbar(t)\hbar(t')} \sum_{\alpha, \beta = \pm} \alpha\beta \left( \frac{1}{N} \boldsymbol{\sigma}^\alpha(t) \boldsymbol{\sigma}^\beta(t') \right)^p \quad (15)$$

where  $\alpha, \beta = \pm$  are the Schwinger-Keldysh contours.

### E. Transformed Order Parameters

The quadratic part of the action may be written in matrix form as:

$$S_{eff}^{(2)}[\boldsymbol{\sigma}^+, \boldsymbol{\sigma}^-] = -\frac{1}{2} \int dt dt' \boldsymbol{\sigma}^\alpha(t) O_p^{\alpha\beta}(t, t') \boldsymbol{\sigma}^\beta(t') \quad (16)$$

where the matrix elements are given by:

$$O_p^{++}(t, t') = \frac{1}{\hbar(t)} [m\partial_t^2 + z^+(t)] \delta(t - t') - \frac{2}{\hbar_0} (i\nu(t - t') - \eta(t - t')) \Theta(t - t_q) \Theta(t' - t_q), \quad (17)$$

$$O_p^{+-}(t, t') = \frac{1}{\hbar_0} (2\eta(t - t') + 2i\nu(t - t')) \Theta(t - t_q) \Theta(t' - t_q), \quad (18)$$

$$O_p^{-+}(t, t') = \frac{1}{\hbar_0} (-2\eta(t - t') + 2i\nu(t - t')) \Theta(t - t_q) \Theta(t' - t_q), \quad (19)$$

$$O_p^{--}(t, t') = -\frac{1}{\hbar(t)} [m\partial_t^2 + z^-(t)] \delta(t - t') - \frac{2}{\hbar_0} (i\nu(t - t') + \eta(t - t')) \Theta(t - t_q) \Theta(t' - t_q). \quad (20)$$

We now introduce new variables  $Q^{\alpha\beta}(t, t')$  (where  $\alpha, \beta = \pm$ ) which will allow us to decouple the  $p$ -interaction term:

$$1 = \int \prod_{\alpha\beta} \mathcal{D}Q^{\alpha\beta} \delta \left( \frac{1}{N} \boldsymbol{\sigma}^\alpha(t) \boldsymbol{\sigma}^\beta(t') - Q^{\alpha\beta}(t, t') \right), \quad (21)$$

$$\propto \int \prod_{\alpha\beta} \mathcal{D}Q^{\alpha\beta} \mathcal{D}\lambda^{\alpha\beta} \exp \left( -\frac{i}{2} \lambda^{\alpha\beta} (\boldsymbol{\sigma}^\alpha(t) \boldsymbol{\sigma}^\beta(t') - N Q^{\alpha\beta}(t, t')) \right). \quad (22)$$

### F. Saddle-Point Equations

Following the notation of Ref. 1, we can define the following matrices:

$$\Lambda(t, t') = \begin{bmatrix} \lambda^{++}(t, t') & \lambda^{+-}(t, t') \\ \lambda^{-+}(t, t') & \lambda^{--}(t, t') \end{bmatrix}, \quad \mathcal{Q}(t, t') = \begin{bmatrix} Q^{++}(t, t') & Q^{+-}(t, t') \\ Q^{-+}(t, t') & Q^{--}(t, t') \end{bmatrix} \quad (23)$$

to allow us to compactly encode all correlations between contours. Further, since taking derivatives of the action with respect to  $Q$  will naturally lead to terms of the form  $Q^{p-1}$ , we also need to define the matrix:

$$F[Q](t, t') = \begin{bmatrix} [Q^{++}(t, t')]^{p-1} & -[Q^{+-}(t, t')]^{p-1} \\ -[Q^{-+}(t, t')]^{p-1} & [Q^{--}(t, t')]^{p-1} \end{bmatrix} \frac{\mathcal{J}(t)\mathcal{J}(t')}{\hbar(t)\hbar(t')} \quad (24)$$

where the time-dependent parameters  $\mathcal{J}(t)$  and  $\hbar(t)$  are included in the definition of  $F[Q]$  as it is necessary to keep track of these time-dependences throughout the following procedure. In this notation, the saddle point equation with respect to  $\Lambda(t, t')$  is given by:

$$i\Lambda(t, t') = \mathcal{Q}^{-1}(t, t') - iO_p(t, t') \quad (25)$$

And with respect to  $\mathcal{Q}(t, t')$ :

$$i\Lambda(t, t') = \frac{p}{2} F[Q](t, t') \quad (26)$$



We can combine these two saddle-point equations to eliminate the variable  $\Lambda$  and obtain:

$$\mathcal{Q}^{-1}(t, t') - iO_p(t, t') = \frac{p}{2}F[Q](t, t') \quad (27)$$

Multiplying from the right with the matrix  $\mathcal{Q}$  results in the final equation:

$$iO_p \otimes \mathcal{Q}(t, t') = \mathcal{I} - \frac{p}{2}F[Q] \otimes \mathcal{Q}(t, t') \quad (28)$$

where the  $\otimes$  symbol denotes the operational product and we have defined  $\mathcal{I} = \mathcal{I}^{\alpha\beta}(t, t') = \delta_{\alpha\beta}\delta(t - t')$ . The saddle-point equations with respect to the Lagrange multiplier  $z^\alpha$  reduce to the definition of the spherical constraint on both contours, and are not shown explicitly here.

### G. Dynamical Equations

We can express both  $C(t, t')$  and  $R(t, t')$  in terms of appropriate sums over  $Q^{\alpha\beta}(t, t')$ , and so the dynamical equations for these variables can be obtained from the saddle-point equations. Specifically:

$$R(t, t') = \frac{i}{\hbar(t')} [Q^{++}(t, t') - Q^{+-}(t, t')] \quad (29)$$

and so the dynamical equation for the response function follows from subtracting the  $++$  and  $+-$  components of Eq. 28. Note that the time-dependent  $\hbar(t)$  presents a complication with respect to the derivation of Ref. 1, and that adding together these components of Eq. 28 gives:

$$\left(\frac{\hbar(t')}{\hbar(t)}\right) [m\partial_t^2 + z(t)]R(t, t') = \delta(t - t') + \left(\frac{\hbar(t')}{\hbar(t)}\right) \int_0^t dt'' \Sigma(t, t'')R(t'', t') \quad (30)$$

where the self-energy  $\Sigma(t, t')$  is defined below. Multiplying through by  $\hbar(t)/\hbar(t')$  and using that  $(\hbar(t)/\hbar(t'))\delta(t - t') = \delta(t - t')$ , we recover the same dynamical equation as in Ref. 1. Similarly, the correlation function is given by:

$$C(t, t') = \frac{1}{2} [Q^{+-}(t, t') + Q^{-+}(t, t')] \quad (31)$$

the dynamical equation for which is obtained from the addition of the  $+-$  and  $-+$  components of Eq. 28. The detailed derivation follows the steps of Ref. 1 with no additional complications and as such is not reproduced here.

### H. Final Dynamical Equations

We can write both dynamical equations in a compact form as:

$$[m\partial_t^2 + z(t)]R(t, t') = \delta(t - t') + \int_0^t dt'' \Sigma(t, t'')R(t'', t'), \quad (32)$$

$$[m\partial_t^2 + z(t)]C(t, t') = \int_0^t dt'' \Sigma(t, t'')C(t'', t') + \int_0^{t'} dt'' D(t, t'')R(t', t'') \quad (33)$$

where we have defined the self-energy  $\Sigma(t, t')$  and the vertex  $D(t, t')$  as the following:

$$\Sigma(t, t') = -4\eta(t - t')\Theta(t - t_q)\Theta(t' - t_q) - \frac{p\mathcal{J}(t)\mathcal{J}(t')}{\hbar(t')} \text{Im} \left[ C(t, t') - \frac{i\hbar(t')}{2}R(t, t') \right]^{p-1}, \quad (34)$$

$$D(t, t') = 2\hbar_0\nu(t - t')\Theta(t - t_q)\Theta(t' - t_q) + \frac{p\mathcal{J}(t)\mathcal{J}(t')}{2} \text{Re} \left[ C(t, t') - \frac{i}{2}(\hbar(t')R(t, t') + \hbar(t)R(t', t')) \right]^{p-1}. \quad (35)$$

From the structure of the saddle-point equations, we can also obtain the equal-time relations:

$$C(t, t) = 1 \quad \partial_t C(t, t')|_{t' \rightarrow t^-} = \partial_t C(t, t')|_{t' \rightarrow t^+} = 0 \quad (36)$$

$$R(t, t) = 0 \quad \partial_t R(t, t')|_{t' \rightarrow t^-} = \frac{1}{m} \quad \partial_t R(t, t')|_{t' \rightarrow t^+} = 0. \quad (37)$$

At this point, we have the equations for the evolution of the correlation and response functions, but we need to perform this evolution subject to the time-dependent Lagrange multiplier  $z(t)$  which is used to enforce the global spherical constraint at all times. We obtain the dynamical equation for  $z(t)$  by taking the  $t' \rightarrow t^-$  limit of Eq. 33 above:

$$z(t) = \int_0^t dt'' [\Sigma(t, t'')C(t'', t) + D(t, t'')R(t, t'')] - m\partial_t^2 C(t, t')|_{t' \rightarrow t^-} \quad (38)$$

## II. NUMERICAL CONSIDERATIONS

The equations of motion can be straightforwardly discretised and solved numerically, however for an isolated system numerical errors can lead to a violation of energy conservation, with an error that increases in time proportionally with the step size  $\delta t$ . This error can prevent the numerical algorithm from reaching long times after the second quench. We overcome this problem by following the procedure of Ref. 2 and replacing the second-derivative term in  $z(t)$  by an energy density:

$$z(t) = \frac{(p+2)}{p} \int_0^t dt'' [\Sigma(t, t'')C(t'', t) + D(t, t'')R(t, t'')] + 2E(t) \quad (39)$$

where  $E(t) = E_k(t) + E_p(t)$  is the total energy density of the system. For the isolated system, we can fix  $E(t)$  immediately following the second quench, which enforces energy conservation and allows us to reach long times while maintaining reasonable numerical accuracy. This can be derived in the following way. The kinetic energy is given by:

$$E_k = \frac{m}{2} \sum_i \langle \dot{\sigma}_i(t)^2 \rangle = -\frac{m}{2} \partial_t^2 C(t, t')|_{t' \rightarrow t^-} \quad (40)$$

as discussed in Ref 2. The potential energy density<sup>4</sup> is given by<sup>3</sup>:

$$E_p = -\frac{1}{N} \left\langle \left\langle \mathcal{J}(t) \sum_{i_1 \dots i_p} J_{i_1 \dots i_p} \sigma_{i_1}(t) \dots \sigma_{i_p}(t) \right\rangle \right\rangle = \frac{1}{p} \int_0^\infty dt' [\Sigma(t, t')C(t, t') + D(t, t')R(t, t')] \quad (41)$$

and by combining these two expressions and using that the total energy is  $E(t) = E_k(t) + E_p(t)$ , we can rewrite the Lagrange multiplier and obtain the expression above. For the classical system, we checked numerically that these quantities reproduce known classical results. For the quantum system, we verified that the resulting energy matches that obtained with free unconstrained time-evolution for short periods following the second quench, before the numerical error becomes significant.

## III. FLUCTUATION-DISSIPATION THEOREM

The quantum fluctuation-dissipation relation for an equilibrium system is:

$$R(\tau) = \frac{2i}{\hbar} \Theta(\tau) \int_{-\infty}^{\infty} \frac{d\omega}{2\pi} \exp[-i\omega\tau] \tanh\left(\frac{\beta\hbar\omega}{2}\right) C(\omega) \quad (42)$$

where  $C(\omega)$  is the Fourier transform of the (time-translation invariant) correlation function  $C(\tau)$  with  $\tau = t - t'$ . In the case where  $\beta\hbar\omega/2 \ll 1$ , i.e. in the limits of high temperature, low frequency or  $\hbar \rightarrow 0$ , we recover the classical result:

$$R(\tau) = -\frac{1}{T} \frac{dC(\tau)}{d\tau}. \quad (43)$$

The generalised quantum fluctuation-dissipation theorem for a system out of equilibrium<sup>1</sup> is given by:

$$R(t, t') = \frac{2i}{\hbar} \Theta(t - t') \int_{-\infty}^{\infty} \frac{d\omega}{2\pi} \exp[-i\omega(t - t')] \tanh\left(\frac{\beta_{eff}\hbar\omega}{2}\right) C(t, \omega) \quad (44)$$

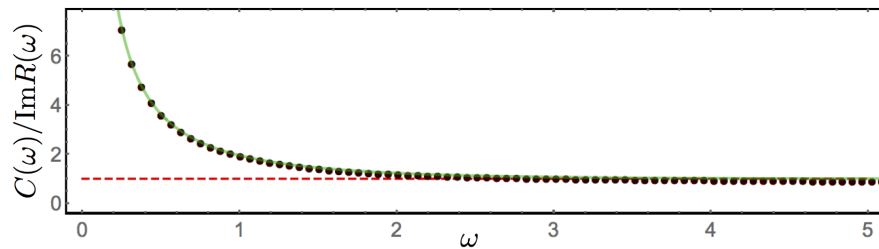


FIG. 1: The ratio  $C(t, \omega)/\text{Im}[R(t, \omega)]$  computed numerically (black dots) and fitted with a function of the form shown in Eq. 46 (green solid line) for a system coupled to a bath with  $t_{max} = 100$ ,  $dt = 0.006\hat{\phi}$ ,  $\mathcal{J} = 1$ ,  $T_{bath} = 1.0$  and  $\hbar = 1.0$ . The red dashed line is a guide to the eye at  $\lim_{y \rightarrow \infty} \coth y = 1$ . We see that the numerical data is very well fitted by the coth function and quantum FDT holds.

where  $\beta_{eff} = 1/T_{eff}$  is the inverse effective temperature and

$$C(t, \omega) = 2\text{Re} \int_0^t dt'' \exp[i\omega(t - t'')] C(t, t'') \quad (45)$$

is a partial Fourier transform of the correlation function. In principle, the effective temperature is a function of both times  $t$  and  $t'$  as well as  $\hbar(t)$ , however we suppress this dependence for clarity of presentation.

To check that our system is well-equilibrated before we cut off the bath and perform the second quench, we can compute the Fourier-transformed correlation and response. From the above quantum FDT relation, the ratio of these is given by:

$$\frac{C(t, \omega)}{\text{Im}[R(t, \omega)]} = \hbar \coth\left(\frac{\beta^* \hbar \omega}{2}\right) \quad (46)$$

We can compute this ratio numerically and fit it with a coth function to extract the temperature of the system: results are shown in Fig. 1. We see very good agreement between the quantum FDT and the numerical data, confirming that in equilibrium, our numerical procedure behaves as expected.

After the second quench, the system is manifestly out of equilibrium and the FDT only holds for the low-frequency degrees of freedom. Following the results of Ref. 1 who showed that the correlation and response of the quantum system in the aging regime are related in a remarkably similar way to the classical FDT, we use a generalisation of the classical result (Eq. 43) with  $T \rightarrow T_{eff}$ . To extract this temperature, it is convenient to define the integrated response:

$$\chi(t, t') = \int_{t'}^t dt'' R(t, t''). \quad (47)$$

For a classical system in equilibrium, a plot of  $\chi(t, t')$  against  $C(t, t')$  will be a straight line with gradient  $-1/T$ . Violations of FDT will result in a deviation away from a straight line and often a visible separation of time scales, however we can still use this relation to extract an effective temperature in the long-time limit.

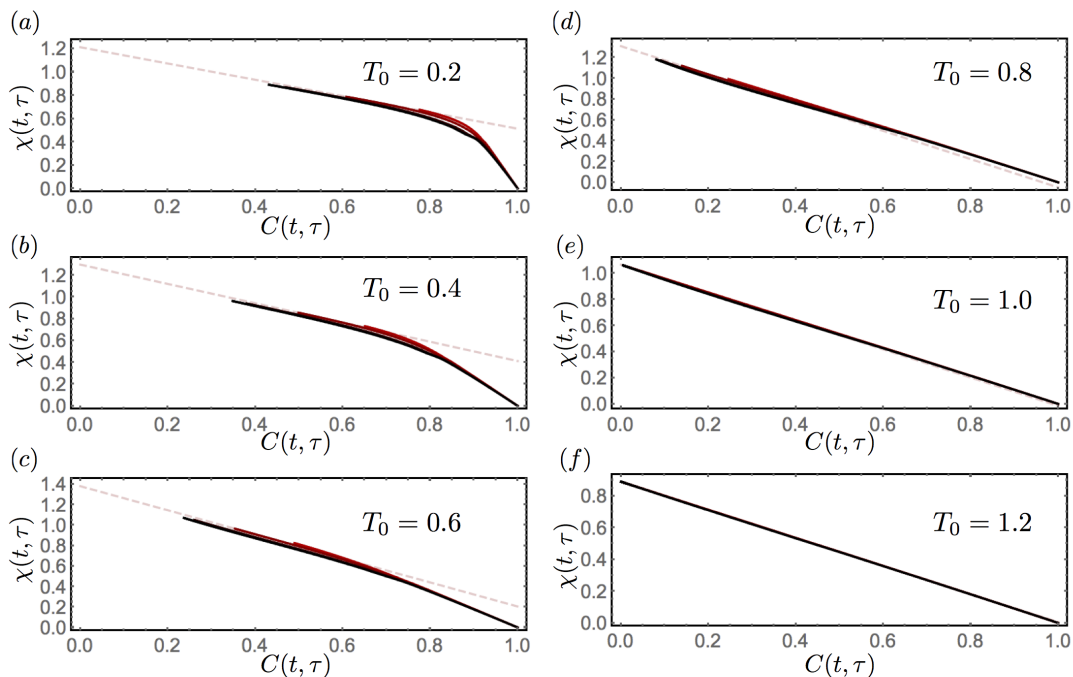


FIG. 2: The integrated response  $\chi(t, \tau)$  of the classical  $p$ -spin model plotted parametrically against the correlation function  $C(t, \tau)$  for a variety of  $\tau = 5, 6.25, 12.5, 20$  (from black to red respectively). In the left column, the system is in the glass phase: time-translation invariance is broken and the FDT shows the clear existence of two time scales, each characterised by a different effective temperature (i.e. slope of the line). In the right column, the system is in the paramagnetic phase: the plots display time-translation invariance and the curves lie on top of one another. At  $T_0 = 0.8$ , the system is paramagnetic but close to the transition: the dynamics in this regime are extremely slow, reflected by the waiting-time dependence starting to emerge at long times. All data were taken with  $t_{max} = 50$  and  $\delta t = 0.0066$ .

## IV. EQUILIBRATION

### A. Equilibration with a bath

In order to establish the accuracy of the double-quench protocol, we first test the quality of the initial equilibration step by using the FDT to extract the temperature of the system in the time window  $0 < t < t_q$  and check that it reproduces known features of the equilibrium system. The integrated response plotted against the correlation function for a variety of wait times and bath temperatures are shown in Fig. 2, in the well-studied classical case of  $\hbar_0 = 0$ . We see that in the paramagnetic phase, the system displays time-translation invariance (TTI) and obeys classical equilibrium FDT, whereas at low temperature, the FDT is violated and there is a clear separation of time scales: an early-time transient regime which displays time-translational invariance, followed by the onset of an aging regime where TTI is broken and the system is no longer in equilibrium.

### B. Effective Temperature

In Fig. 3, we show the effective temperature extracted from the equilibrium FDT relation plotted against the bath temperature, for two different maximum times  $t_{max} = 50$  (with  $N = 7500$ ) and  $t_{max} = 100$  ( $N = 15,000$ ) in blue and red respectively. We see that the dependence on  $t_{max}$  is slight, giving us good confidence that the pre-quench equilibration used in the main text is sufficiently accurate. In the paramagnetic phase, the error  $\Delta T = T_0 - T_{eff}$  is controlled predominantly by the step-size  $\delta t$  used - we typically use  $\delta t = 0.0066$  in order to obtain a good compromise between retaining numerical accuracy and being able to reach a suitably large  $t_{max}$ .

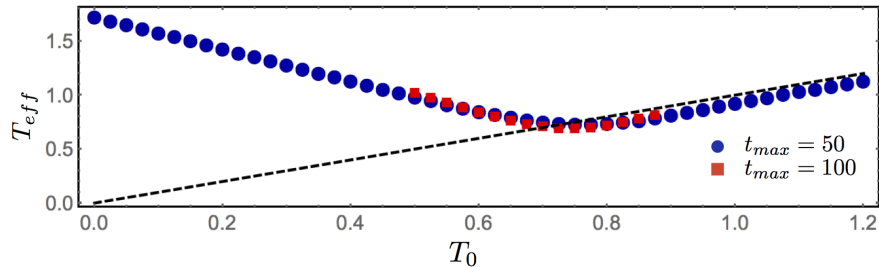


FIG. 3: The effective temperature  $T_{eff}$  obtained from the FDT relation plotted against the bath temperature  $T_0$ . The black dashed line is a guide to the eye with slope equal to one. Both sets of data points use the same step size ( $\delta t = 0.0066$ ). Note the non-monotonic behaviour of  $T_{eff}$  on crossing the phase transition from above: this feature can be used to identify a transition temperature from the numerical data.

A key feature of Fig. 3 is the non-monotonic behaviour of the effective temperature  $T_{eff}$ , which rises sharply as the bath temperature decreases and we pass through the phase transition. This behaviour has been seen in a variety of other works, most notably Ref. 2. In the present work, we take the minimum value of the effective temperature  $T_{eff}^*$  to indicate the phase transition in our numerical data; this is how we compute the equilibrium phase boundary shown in the main text. The true temperature of the equilibrium phase transition in the classical  $p$ -spin model is  $T_d \approx 0.6$ . Due to the finite timescale of our simulation and the increasingly slow dynamics on approach to the transition, the transition in our data occurs at a slightly higher bath temperature: this is symptomatic of the difficulties in extracting a glassy phase transition from dynamical data taken on finite timescales. We expect this finite-time error to result in a small systematic shift of all of our results, but to have no qualitative effect.

### C. Equilibration of the isolated system

After the second quench, the system is out of equilibrium but we can still use the generalised FDT in the low-frequency limit to extract an effective temperature. Representative plots of the integrated response for a system equilibrated with a classical bath at  $T_0 = 0.8$  are shown in Fig. 4. For small quenches in  $\hbar_F$ , the system remains in equilibrium and continues to obey the classical FDT, as evidenced by Fig. 4(a). As we increase  $\hbar_F$ , the system enters an aging regime and no longer obeys classical FDT. To extract an effective temperature, we fit the late-time part of the  $\chi$  vs  $C$  curve: the results of this are shown in the main text.

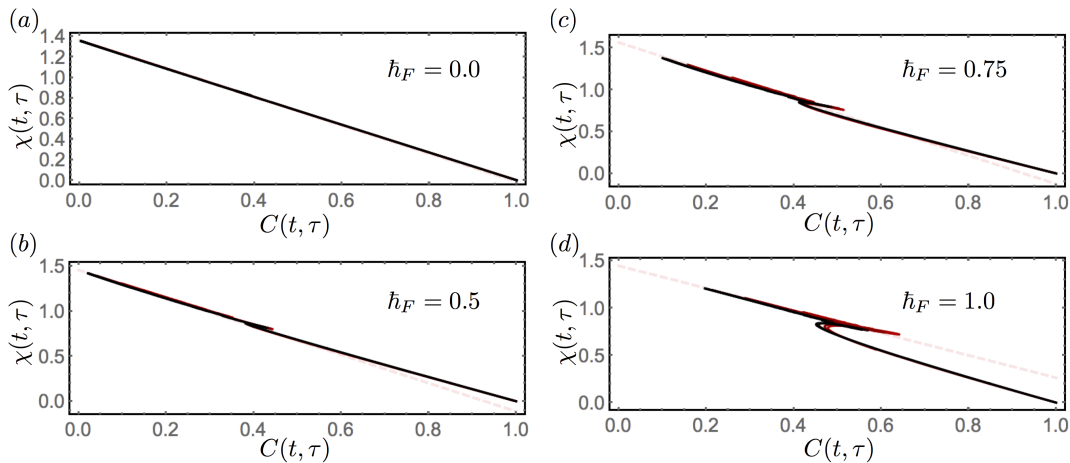


FIG. 4: The same quantities as Fig. 2, but now after the second quench. In each case, the system was first equilibrated at a temperature  $T_0 = 0.8$  with  $\hbar_0 = 0.0$ . For small  $\hbar_F$ , the system continues to respect the classical FDT and the plots are approximately straight lines, however as  $\hbar_F$  increases above the transition at approximately  $\hbar_F \approx 0.7$ , we see that the system violates classical FDT and the parametric plots take a highly non-trivial form with two distinct time sectors.

- 
- <sup>1</sup> L. F. Cugliandolo and G. Lozano, Phys. Rev. B **59**, 915 (1999).
- <sup>2</sup> L. F. Cugliandolo, G. S. Lozano, and E. N. Nessi, Journal of Statistical Mechanics: Theory and Experiment **2017**, 083301 (2017).
- <sup>3</sup> L. F. Cugliandolo, G. Lozano, and H. Lozza, The European Physical Journal B - Condensed Matter and Complex Systems **41**, 87 (2004).
- <sup>4</sup> Note that in the case of a system-bath coupling, the bath contributions must be subtracted from the self-energy  $\Sigma(t, t')$  and vertex  $D(t, t')$  shown here.